

# Communication-Efficient TeraByte-Scale Model Training Framework for Online Advertising

Weijie Zhao<sup>1</sup>, Xuewu Jiao<sup>2</sup>, Mingqing Hu<sup>2</sup>, Xiaoyun Li<sup>1</sup>, Xiangyu Zhang<sup>2</sup>, Ping Li<sup>1</sup>

<sup>1</sup> Cognitive Computing Lab, Baidu Research

<sup>2</sup> Baidu Search Ads (Phoenix Nest), Baidu Inc.

10900 NE 8th St. Bellevue, Washington 98004, USA

No. 10 Xibeiwang East Road, Beijing 100193, China

{weijiezhao jiaoxuewu humingqing, xiaoyunli, zhangxiangyu06, liping11}@baidu.com

## Abstract

Click-Through Rate (CTR) prediction is a crucial component in the online advertising industry. In order to produce a personalized CTR prediction, an industry-level CTR prediction model commonly takes a high-dimensional (e.g., 100 or 1000 billions of features) sparse vector (that is encoded from query keywords, user portraits, etc.) as input. As a result, the model requires Terabyte scale parameters to embed the high-dimensional input. Hierarchical distributed GPU parameter server has been proposed to enable GPU with limited memory to train the massive network by leveraging CPU main memory and SSDs as secondary storage. We identify two major challenges in the existing GPU training framework for massive-scale ad models and propose a collection of optimizations to tackle these challenges: (a) the GPU, CPU, SSD rapidly communicate with each other during the training. The connections between GPUs and CPUs are non-uniform due to the hardware topology. The data communication route should be optimized according to the hardware topology; (b) GPUs in different computing nodes frequently communicates to synchronize parameters. We are required to optimize the communications so that the distributed system can become scalable.

In this paper, we propose a hardware-aware training workflow that couples the hardware topology into the algorithm design. To reduce the extensive communication between computing nodes, we introduce a  $k$ -step model merging algorithm for the popular Adam optimizer and provide its convergence rate in non-convex optimization. To the best of our knowledge, this is the first application of  $k$ -step adaptive optimization method in industrial-level CTR model training. The numerical results on real-world data confirm that the optimized system design considerably reduces the training time of the massive model, with essentially no loss in accuracy.

All experiments are conducted on Baidu's ads production system which is part of the PaddlePaddle deep learning platform. <https://www.paddlepaddle.org.cn>

# 1 Introduction

Online advertising industry displays sponsored ads in the searching results and recommendations, and profits from the ads publisher whenever the displayed ad is clicked. Baidu ([www.baidu.com](http://www.baidu.com)) has developed over the past two decades a mature and powerful advertising system (a.k.a. “Phoenix Nest”) that makes a handsome profit for the corporation. As reviewed in (e.g.) [Fan et al. \(2019\)](#); [Zhao et al. \(2020\)](#), Baidu started to use distributed parameter servers for massive scale logistic regression around 2010 and launched their distributed deep learning training system in production around 2013. An important task in the ads system is to train machine learning models for Click-Through-Rate (CTR) prediction ([Broder, 2002](#); [Fain and Pedersen, 2006](#)). CTR measures the number of click-throughs per ad display—it is employed to quantify the performance of an ad display strategy. Thus, CTR prediction becomes one of the most crucial components in the online advertising industry, in which the prediction accuracy directly affects the revenue. In recent years, at Baidu Search Ads, multiple directions has been taken to improve the performance of CTR prediction, including using approximate near neighbor search for improving recalls ([Fan et al., 2019](#); [Zhou et al., 2019](#)), GPU-based ads production systems ([Zhao et al., 2019, 2020](#)), model compression ([Xu et al., 2021](#)), etc.

In the early stage of this line of research, data scientists used classical regression algorithms, e.g., logistic regression and gradient boosting, for CTR prediction ([Edelman et al., 2007](#); [Graepel et al., 2010](#)). In recent years, deep learning, which could achieve state-of-the-art performance in numerous tasks, has attracted great attention in both industry and academia. With the rapid development of computing resources (e.g. GPU), machine learning researchers have applied large models with a massive number of parameters in practice to achieve higher learning accuracy ([Shan et al., 2016](#); [Covington et al., 2016](#); [Zhou et al., 2018b](#); [Qu et al., 2016](#)). For CTR prediction, in this paper, we consider extremely sparse input which encodes the query keywords, user portrait, etc. The sparse input vector is first embedded into a low-dimensional ( $\sim 100$ ) dense representation and then fed to subsequent network components, i.e., attention component and multi-layer perceptron. Because of the ultra-high dimensionality of the input layer, the CTR model requires a massive number of parameters ( $>10$  TB).

Besides achieving high accuracy, it is also important for practitioners to be able to train the large CTR model in an efficient manner. This is because: 1) the CTR prediction model should be capable of incorporating the continuously changing information; 2) machine learning researchers may need to rapidly train CTR models for evaluation and strategy development. In order to tackle the massive-scale learning problem, in industrial applications, people commonly resort to a distributed parameter server ([Valiant, 1990](#); [Ho et al., 2013](#); [Huang et al., 2018](#)) across a computing cluster, with dozens to hundreds of nodes. However, training in a large computing cluster requires significant communications and synchronizations that limit the efficiency of the training task. Recently, to reduce the communications, distributed GPU parameter servers ([Zhao et al., 2020](#)) are introduced to train massive-scale models on a handful of nodes accelerated by GPUs and SSDs.

Nonetheless, previous studies focus on effectively using CPU main memory and SSDs to handle out-of-GPU-memory scenarios. When the model becomes more complicated and requires more computing nodes, the communication issue will still exist and slow down the training process.

**Challenges & approaches.** We identify two major challenges in the design of GPU-SSD accelerated training framework: local communication inside a computing node and network communications among nodes. First, GPUs in the same computing node are required to rapidly communicate with each other to sum up the gradients and synchronize the parameters. Thus, the speed of transmitting gradients/parameters become crucial. However, it is non-trivial to perform the collective

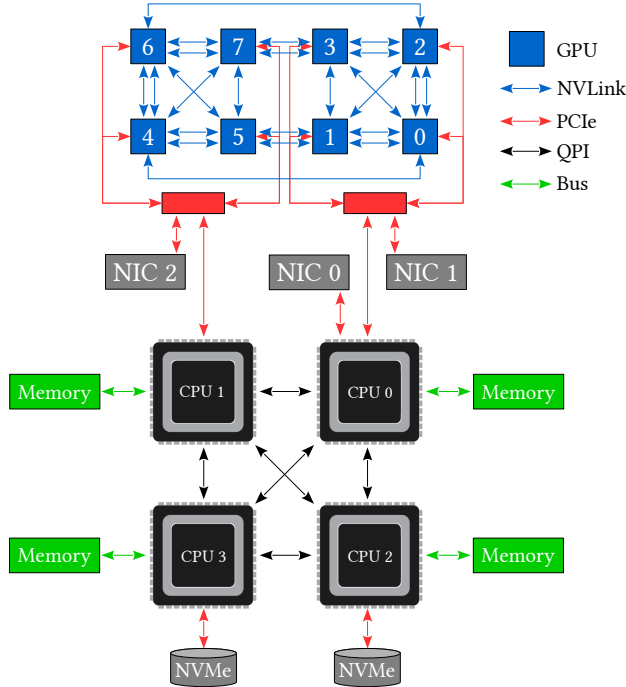


Figure 1: An example hardware topology of a GPU node.

reduction/broadcast in a real system because of the hardware topology: the bandwidths between GPUs are not identical. For example, in Figure 1, GPU 0, 1, 2, and 3 are on one socket while the other 4 GPUs (4, 5, 6, and 7) locate on the other socket. Since GPU 1, 3, 5, and 7 need to connect the GPUs across two sockets, their bandwidths to the GPUs in their own socket are reduced: e.g., the link between GPU 0 and 2 has 2X bandwidth than the link between GPU 1 and 3. Even in the same socket, the bandwidths between two GPUs are now the same: e.g., GPU 0 and GPU 3 have only one NVLink bridge connector between them so that it has only half bandwidth than the one between GPU 0 and 2. A standard collective reduction/broadcast is not aware of the hardware topology and thus yields suboptimal performance. We allocate the I/O workload onto the CPU cores that are co-located to the I/O device to reduce the data transferring across NUMA sockets. Also, GPU, CPU, and SSDs in the same node rapidly communicate during the training to load/cache/dump sparse parameters. The communications are required to be optimized so that the inner-node I/O does not become a bottleneck of the training framework.

The second challenge is the communication between the computing nodes. Although GPU RDMA is discussed in Zhao et al. (2020), the inter-node communication through the network is slow and has incomparable bandwidth with the inner-node PCI-E data transfer—frequent inter-node synchronizations hurt the training performance. We introduce a  $k$ -step model merging algorithm with Adam (Kingma and Ba, 2015) as the local optimizer, which is different from the common local SGD ( $k$ -step SGD) in that Adam employs adaptive coordinate-wise learning rates during the training process.

**Contributions.** Specifically, our contributions include:

- We propose a hardware-aware training workflow that couples the hardware topology into the algorithm design. The proposed techniques have been implemented in our real-world ads system and obtained a good success in our company. We believe these engineering details would be interesting to the machine learning community.
- To reduce the extensive communication between computing nodes, we introduce a  $k$ -step model merging algorithm for Adam and provide its convergence rate in non-convex optimization. To the best of our knowledge, this is the first application of  $k$ -step adaptive optimization in industrial-level CTR model training.
- We experimentally evaluate the proposed system on real-world ads data. The empirical results confirm the effectiveness of our proposed optimizations.

## 2 Preliminaries

In this section, we introduce the CTR prediction model and the distributed GPU parameter server. Both concepts are the foundations of the proposed framework in this paper.

### 2.1 CTR Prediction Model

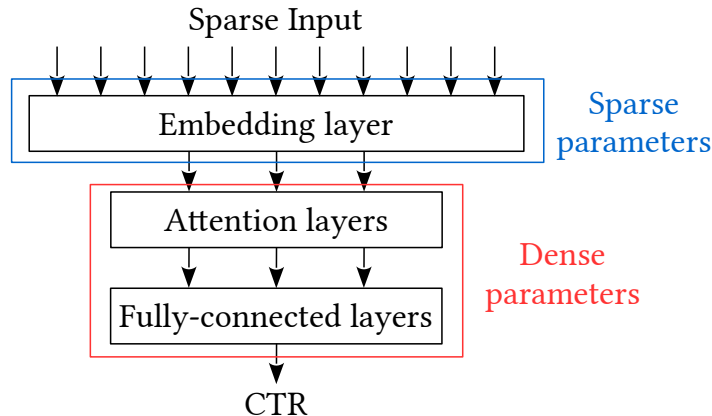


Figure 2: An example structure of our CTR prediction model.

Given an ad, we target to use a CTR prediction model to predict the probability that the ad will be clicked based on a variety of input sources, e.g., search keywords, user portrait, and more ad features. Those input sources are commonly encoded in a one-hot/multi-hot representation—the input vector is formalized as an extremely sparse vector with  $\sim 10^{11}$  dimensions and only  $\sim 100$  non-zeros on average. Figure 2 depicts an example neural network architecture of a commercial CTR prediction model. The ultra-high dimensional vector is fed to an embedding layer to produce a low-dimensional representation. After that, more complicated neural network components, such as attention and fully-connected layers (Shan et al., 2016; Cheng et al., 2016; Covington et al., 2016; Qu et al., 2016; Guo et al., 2017; Lian et al., 2018), are employed on the low-dimensional embedding to predict the CTR.

## 2.2 Why Not Using Hashing?

This is the same question the authors were asked over and over in the past years. We have answered it thoroughly in [Zhao et al. \(2020\)](#), that commercial search engines are unable to tolerate any noticeable (e.g., 0.1%) loss of accuracy which directly impact the revenues.

Nevertheless, here we present the same [Table 1](#) taken from [Zhao et al. \(2020\)](#), for reporting the previous efforts (since 2015) in developing hashing methods for online ads system for web search. As we can see, the baseline deed learning model (“Baseline DNN”) achieved an AUC of 0.7670. Although hashing substantially reduced the model size, it is not realistic to replace the current production system because the loss of accuracy is not acceptable, even though the loss appears very small from academic perspective.

Table 1: OP+OSRP hashing for Web Search Sponsored Ads Data, taken from [Zhao et al. \(2020\)](#)

	# Nonzero Weights	Test AUC
Baseline LR	199,359,034,971	0.7458
Baseline DNN		0.7670
Hash+DNN (k = 2 <sup>32</sup> )	3,005,012,154	0.7556
Hash+DNN (k = 2 <sup>31</sup> )	1,599,247,184	0.7547
Hash+DNN (k = 2 <sup>30</sup> )	838,120,432	0.7538
Hash+DNN (k = 2 <sup>29</sup> )	433,267,303	0.7528
Hash+DNN (k = 2 <sup>28</sup> )	222,780,993	0.7515
Hash+DNN (k = 2 <sup>27</sup> )	114,222,607	0.7501
Hash+DNN (k = 2 <sup>26</sup> )	58,517,936	0.7487
Hash+DNN (k = 2 <sup>24</sup> )	15,410,799	0.7453
Hash+DNN (k = 2 <sup>22</sup> )	4,125,016	0.7408

## 2.3 Distributed Hierarchical GPU Parameter Server

Currently, the off-the-shelf GPU with the largest memory capacity has 40 GB High-Bandwidth Memory (HBM). Comparing with the 10 TB parameters of CTR models, GPUs have too limited HBM to hold the massive-scale parameters. To tackle this challenge, distributed hierarchical GPU parameter server is introduced in [Zhao et al. \(2020\)](#). The key observation made this possible is that: the input is extremely sparse (only hundreds of non-zeros)—only hundreds of parameters in the massive-scale embedding layer are referenced and required to be loaded during the feed forward and back propagation. Therefore, the working parameters in a mini-batch fit in the GPU memory. [Zhao et al. \(2020\)](#) maintains a distributed hash table in the HBM across GPUs to store the working parameters and use CPU main memory and NVMe SSDs as secondary storage.

**Training workflow.** Algorithm 1 illustrates the distributed hierarchical parameter server training workflow. The training data batches are streamed into the main memory through the network card (NIC 0 in [Figure 1](#)) with a network file system, e.g., HDFS (line 2). The parallel training framework falls in the data-parallel category ([Li et al., 2014](#); [Cui et al., 2014, 2016](#); [Luo et al., 2018](#)). Each computing node processes its own training batches—different nodes receive different training data from HDFS. The streamed data for different nodes are in an i.i.d. distribution. Then, each node identifies the union of the referenced parameters in the current received batch and pulls these parameters from the local memory/SSD and its peer computing nodes (line 3). The local in-memory cache management loads the local parameters stored on SSDs into the memory

---

**Algorithm 1** Training Workflow

---

```
1. while not converged do
2.   batch  $\leftarrow$  read_batch_from_network()
3.   working  $\leftarrow$  pull_parameters(batch)
4.   minibatches  $\leftarrow$  shard_batch(batch, #GPU, #minibatch)
5.   part  $\leftarrow$  partition_parameters_to_GPUs(working, #GPU)
6.   for i  $\leftarrow$  1 to #GPU do
7.     transfer_to_GPU(i, minibatchesi)
8.     insert_into_hash_table(i, parti)
9.   end for
10.  for j  $\leftarrow$  1 to #minibatch do
11.    pull_peer_GPU_kernel(minibatchj)
12.     $\Delta_j \leftarrow$  train_mini_batch_kernel(j)
13.    push_parameters_updates_back_kernel( $\Delta_j$ )
14.  end for
15.   $\Delta \leftarrow$  pull_updates_peer_GPU()
16.  parameters_to_dump  $\leftarrow$  update_local_cache()
17.  push_local_SSD(parameters_to_dump)
18. end while
```

---

and requests other nodes for the remote parameters through the network. After we load all the referenced parameters into the memory, these parameters are then partitioned and transferred to the HBM in GPUs. The parameters are partitioned in a non-overlapped fashion to effectively utilize the limited GPU memory. When a GPU worker thread requires the parameter on another GPU, it fetches the parameter from the remote GPU and pushes the updates back to the remote GPU through high-speed inter-GPU hardware connection NVLink (Foley and Danskin, 2017). Then, the data batch is partitioned into multiple mini-batches and fed to each GPU worker thread (line 4-9). An inter-GPU parameter synchronization is performed after each mini-batch. Each training worker pulls the required parameters of its corresponding mini-batch from its peer GPUs (line 11), performs feed forward and backward propagation to update the parameters (line 12), and interacts with its peer GPUs to update the referenced parameters on other GPUs (line 13). A collection of CPU threads collects the updates from the GPU (line 15) and dumps infrequently used parameters to the SSDs when the main memory usage reaches its capacity (line 16-17). GPU HBM, CPU main memory, and SSDs communicate in a hierarchical storage fashion. The upper-level module acts as a high-speed cache of the lower-level module.

### 3 Hardware-Aware Training Framework

#### 3.1 Core Binding

As shown in Figure 1, the physical topology of the system determines the data access path between two devices: GPU 0-3 are connected with the same PCIe slot/switch to CPU 0 while GPU 4-7 are connected to CPU 1; CPU 3 and 4 have connected to an NVMe SSD, respectively. As a result, CPU 0 and 1 have faster access to the GPUs and CPU 2 and 3 have faster SSD access. The 4 CPUs are installed in 4 sockets as the NUMA fashion. The communications between CPUs are transferred through QPI. CPU 2 and 3 connect two 4 NVMe SSDs, respectively. We allocate one physical CPU core for each SSD to manage the I/O: these cores are responsible for loading and

dumping parameters from/to SSDs. The loaded parameters are scattered into the memory of all 4 CPUs—the NUMA memory policy is set to `MPOL_INTERLEAVE` that interleaves page allocations across the CPUs. A network card (NIC 0) is attached to CPU 0 via PCIe to read training data from network file systems. A core in CPU 0 is assigned to solely perform the network I/O. NIC 1 and 2 are controlled by GPUs on the corresponding PCIe switch to perform RDMA GPUDirect I/O with GPUs on other computing nodes. The RDMA communication bypasses the involvement of CPU and main memory access so that we can achieve a larger bandwidth and lower latency.

### 3.2 Two-Phase GPU Communications

During the training workflow described in Algorithm 1, GPUs in the same node rapidly communicates with each other to pull referenced parameters and push update parameters in the distributed hash table across GPUs—the hash table stores the sparse parameters of the embedding layer. However, due to the hardware topology (Figure 1), not all GPUs have direct connections: e.g., GPU 0 cannot directly communicate with GPU 5. In conventional practice, this cross socket communications takes the following route: GPU 0, PCIe switch, CPU0 (memory), QPI, CPU 1 (memory), PCIe switch, and GPU 5. The communication route is inefficient since it involves multiple data copies between CPUs and GPUs.

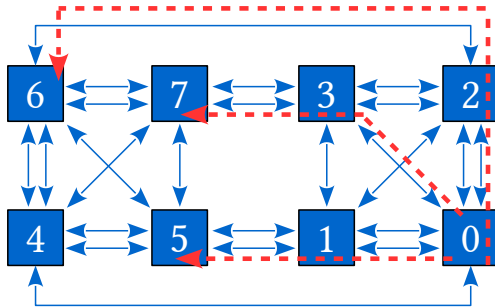


Figure 3: Example two-phase GPU communication patterns.

We propose a two-phase communication strategy to tackle this challenge. The CPU-involved GPU communications only exist when we try to perform cross PCIe socket/switch GPU data transfer without NVLink connection. Figure 3 depicts three representative communication patterns from GPU 0. The communication patterns from other GPUs are similar and thus are omitted. GPU 0 has no NVLink connection with GPU 5, 6, and 7. Instead of routing through CPUs with PCIe switch, we allocate a buffer on GPU 1, 2, and 3, respectively, to forward the data from GPU 0 to 5, 6, and 7. The data transfer route using a middleman GPU to forward the communication eliminates the involvement and data copy of CPU and PCIe switch—the two-phase GPU communications only transfer data through NVLink which has a larger bandwidth.

### 3.3 SSD Direct I/O

By default, common operating systems enable dirty page write back that periodically flush the modified cached pages into the disk. Moreover, a disk cache is also maintained by the operating system in the memory to accelerate the disk access—it always probes the in-memory page cache before accessing disks. However, the hierarchical distributed GPU parameter server has already kept a page cache of parameters. In this case, the system disk cache introduces an unnecessary memory probing overhead. Thus, we disable the dirty page write back and use non-buffered direct disk I/O to access SSDs.



## 4 $k$ -Step Model Merging

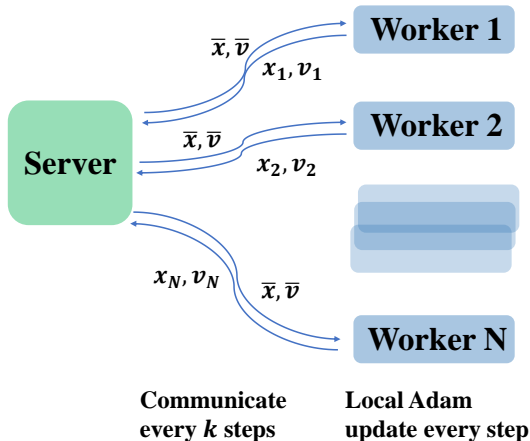


Figure 4: Illustration of distributed  $k$ -step Adam training scheme.

In this section, we introduce our solution to reduce the communication cost among the computing nodes, inspired by the idea of federated learning (McMahan et al., 2017). Note that our CTR model uses Adam (Kingma and Ba, 2015) as the optimizer. In the standard distributed setting, we can average the gradients computed on different nodes in every iteration, and use the averaged gradient for an Adam update. To reduce the communication, instead of communicating in every training iteration, the “local models” are aggregated every  $k$  step, where  $k$  is a positive integer. The pseudocode is summarized in Algorithm 2, with an illustration in Figure 4. On each local worker, standard Adam updates are applied. Every  $k$  iterations, the local machines transmit local model parameters to the central server. The global weight is updated by taking the average of local weights, and then the new global weight is broadcast to local nodes triggering next round of local training. To ensure convergence, the second moment moving average,  $v_t$ , is also averaged in each communication round. To our knowledge, this is the first time a  $k$ -step adaptive optimization method is applied to industrial-scale massive CTR models in literature, which turns out to attain significant communication reduction with good performance (as will be shown in Section 5).

**Communication reduction.** We highlight here the saving in communication of our approach. On a high level, the  $k$ -step merging method differs from standard distributed learning in the frequency of communications. In distributed learning, the server requests the *local gradients* in **every iteration** to update the global model, while the communication in Algorithm 2 only takes place **every  $k$  iterations**, and the *local models* are transmitted, which have same size as the gradients. Naturally, in principle, our method will reduce the communication cost by a factor of  $1/k$ . Typically,  $k$  should not be too large to ensure good learning performance, since local models may deviate from the global model significantly during local training. The requirement on  $k$  can be characterized by the convergence analysis, which will be presented in the remaining part of this section.

In this paper, we consider the finite-sum optimization problem of the form

$$\min_x f(x) := \frac{1}{N} \sum_{i=1}^N f_i(x),$$

where  $N$  is the number of local computing nodes and  $f_i$  is the non-convex loss function evaluated



---

**Algorithm 2**  $k$ -step Adam (with  $N$  workers)

---

```
1: Input: learning rate  $\alpha$ ,  $\beta_1$ ,  $\beta_2$ 
2: Initialize: local models  $x_{0,i}$ , moment estimators  $m_{0,i} = 0$ ,  $v_{0,i} = \epsilon \mathbf{1}$ ,  $i = 1, \dots, N$ 
3: for  $t = 1, \dots, T$  do
4:   Compute stochastic gradient  $g_{t,i} \leftarrow \nabla f_i(x_{t,i}) + \xi_{t,i}$ 
5:    $m_{t,i} = \beta_1 m_{t-1,i} + (1 - \beta_1) g_{t,i}$ 
6:    $v_{t,i} = \beta_2 v_{t-1,i} + (1 - \beta_2) g_{t,i}^2$ 
7:   if  $t \bmod k \neq 0$  then
8:      $v_t = v_{t-1}$ 
9:      $x_{t+1,i} \leftarrow x_{t,i} - \alpha \frac{m_{t,i}}{\sqrt{v_t}}$ 
10:    //Local Adam Update
11:   else
12:      $v_t = \frac{1}{N} \sum_{i=1}^N v_{t,i}$ 
13:      $x_{t+1,i} \leftarrow \frac{1}{N} \sum_{j=1}^N \left( x_{t,j} - \alpha \frac{m_{t,j}}{\sqrt{v_t}} \right)$ 
14:    //Global averaging
15:   end if
16: end for
```

---

over the data on the  $i$ -th node. The following assumptions will be needed:

**A1:**  $f_i$  is differentiable and  $L$ -smooth, i.e.,  $\|\nabla f_i(x) - \nabla f_i(y)\| \leq L\|x - y\|$ ,  $\forall x, y$ .

**A2:** Bounded and unbiased stochastic gradient,  $\mathbb{E}[g_{t,i}] = \nabla f_i(x_{t,i})$ ,  $\|g_{t,i}\|_\infty \leq G$ , and bounded variance,  $\mathbb{E}[(g_{t,i})_j^2] \leq \sigma^2$ ,  $\forall j \in [d]$ .

**A3:**  $\mathbb{E} \left[ \sum_{t=1}^T \left\| \frac{1}{\sqrt{v_{t-1}}} - \frac{1}{\sqrt{v_t}} \right\|_1 \right] \leq Md \cdot T^\gamma$ , with some  $0 \leq \gamma \leq 1/2$  and  $M > 0$ .

Assumption **A1** (Lipschicity) and **A2** (bounded gradients) are standard in the optimization literature. [Chen et al. \(2019\)](#) has shown that the LHS term in **A3** plays an important role in the convergence of Adam-type algorithms. If it is too big, Adam may converge very slowly, or even diverge, in simple optimization problems. Thus, **A3** is to guarantee that the algorithm can converge in a proper manner. In practice, this term is usually very small. The special case  $\gamma = 0$  implies AMSGrad ([Reddi et al., 2018](#); [Chen et al., 2020](#)), a variant of Adam known to have better theoretical convergence behavior, though they perform similarly in practice. In our analysis, we consider **A3** as a more general setting.

**Theorem 1.** Under **A1-A3**, define  $\bar{x}_t = \frac{1}{N} \sum_{i=1}^N x_{t,i}$  and set  $\alpha = \min(\frac{\sqrt{N}}{\sqrt{Td}}, \frac{\sqrt{\epsilon}}{4L})$ . We have

$$\frac{1}{T} \sum_{t=1}^T \mathbb{E} \left[ \left\| \frac{\nabla f(\bar{x}_t)}{v_t^{1/4}} \right\|^2 \right] \leq O\left(\frac{\sqrt{d}}{\sqrt{TN}}\right) + O\left(\frac{d}{T^{1-\gamma}} + \frac{\sqrt{d}N}{T^{1.5-\gamma}}\right) + O\left(\frac{Nk^2}{T}\right).$$

We have simplified many constants for the ease of presentation. The left-hand side of [Theorem 1](#) is a standard metric to measure the convergence speed towards a stationary point in non-convex optimization literature. The dependence on parameter dimension  $d$  is due to the dimension-wise bounds in the assumptions, which can be easily removed by assuming alternative total bounds. We simplify the convergence rate in [Corollary 1](#) when  $k$  is not too large.

**Corollary 1.** Under **A1-A3**, with  $\alpha = \min(\frac{\sqrt{N}}{\sqrt{Td}}, \frac{\sqrt{\epsilon}}{4L})$  and  $k \leq O(T^{1/4}d^{1/4}/N^{3/4})$ ,

$$\frac{1}{T} \sum_{t=1}^T \mathbb{E} \left[ \|\nabla f(\bar{x}_t)\|^2 \right] \leq O\left(\frac{1}{\sqrt{TN}}\right). \quad (1)$$

**Discussion.** From Corollary 1, we see that as long as the number of local updates  $k \leq O(T^{1/4})$ , the convergence rate of  $k$ -step Adam is  $O(\frac{1}{\sqrt{TN}})$ , which matches that of  $k$ -step SGD (FedAvg/LocalSGD) e.g., Zhou and Cong (2018); Yu et al. (2019), and achieves linear speedup compared with vanilla Adam-type method (Zhou et al., 2018a; Chen et al., 2019) w.r.t.  $N$ . For the left-hand side of (1) to achieve  $O(\delta)$ , a single worker needs  $O(1/\epsilon^2)$  iterations, while using  $N$  workers as in  $k$ -step Adam only requires  $O(1/N\epsilon^2)$  iterations, leading to a linear acceleration in training efficiency (in wall-clock time). The condition on  $k$  suggests that, we can attain the same convergence rate of vanilla Adam, with the number of communication rounds sub-linear in  $T$ . Since in our framework the data on each computing node are identically distributed, the  $k$ -step averaging method is expected to work very well empirically, which is a well recognized behavior of federated learning. In the following, we provide a sketch proof of Theorem 1. While the proof is for a new algorithm, we follow the standard procedure in the literature such as Zhou et al. (2018a); Chen et al. (2019, 2020).

**Sketch Proof of Theorem 1:** Define an auxiliary sequence

$$\bar{\theta}_t = \bar{x}_t + \frac{\beta_1}{1 - \beta_1}(\bar{x}_t - \bar{x}_{t-1}).$$

where  $\bar{x}_t = \frac{1}{N} \sum_{i=1}^N x_{t,i}$  and let  $x_0 \triangleq x_1$ . It can be shown that

$$\bar{\theta}_{t+1} - \bar{\theta}_t = \alpha \frac{\beta_1}{1 - \beta_1} \left( \frac{1}{\sqrt{v_{t-1}}} - \frac{1}{\sqrt{v_t}} \right) \odot \bar{m}_{t-1} - \alpha \frac{\bar{g}_t}{\sqrt{v_t}}, \quad (2)$$

where  $\bar{m}_t = \frac{1}{N} \sum_{i=1}^N m_{t,i}$  and  $\bar{g}_t = \frac{1}{N} \sum_{i=1}^N g_{t,i}$ . By **A1**,

$$f(\bar{\theta}_{t+1}) \leq f(\bar{\theta}_t) + \langle \nabla f(\bar{\theta}_t), \bar{\theta}_{t+1} - \bar{\theta}_t \rangle + \frac{L}{2} \|\bar{\theta}_{t+1} - \bar{\theta}_t\|^2.$$

Hence,

$$- \mathbb{E}[\langle \nabla f(\bar{\theta}_t), \bar{\theta}_{t+1} - \bar{\theta}_t \rangle] \leq \mathbb{E}[f(\bar{\theta}_t) - f(\bar{\theta}_{t+1})] + \frac{L}{2} \mathbb{E}[\|\bar{\theta}_{t+1} - \bar{\theta}_t\|^2]. \quad (3)$$

where the expectation is taken over all the randomness of stochastic gradients until iteration  $t$ . By (2), we have

$$\langle \nabla f(\bar{\theta}_t), \bar{\theta}_{t+1} - \bar{\theta}_t \rangle = \alpha \langle \nabla f(\theta_t), \frac{\beta_1}{1 - \beta_1} \left( \frac{1}{\sqrt{v_{t-1}}} - \frac{1}{\sqrt{v_t}} \right) \odot \bar{m}_{t-1} - \alpha \langle \nabla f(\theta_t), \frac{\bar{g}_t}{\sqrt{v_t}} \rangle. \quad (4)$$

Since  $v_t$  is independent of  $\bar{g}_t$  and  $\mathbb{E}[g_{t,i}] = \nabla f_i(x_{t,i})$ , taking expectation on both sides of (4) yields

$$\mathbb{E}[\langle \nabla f(\bar{\theta}_t), \bar{\theta}_{t+1} - \bar{\theta}_t \rangle] = \alpha \mathbb{E} \left[ \langle \nabla f(\theta_t), \frac{\beta_1}{1 - \beta_1} \left( \frac{1}{\sqrt{v_{t-1}}} - \frac{1}{\sqrt{v_t}} \right) \odot \bar{m}_{t-1} \right] - \alpha \mathbb{E} \left[ \langle \nabla f(\theta_t), \frac{\bar{\nabla} f(x_t)}{\sqrt{v_t}} \rangle \right].$$

where  $\bar{\nabla} f(x_t) = \frac{1}{N} \sum_{i=1}^N \nabla f_i(x_{t,i})$ . Denoting the inner product in the second expectation as  $B_1$ , we have

$$B_1 = \frac{1}{2} \left( \left\| \frac{\nabla f(\bar{\theta}_t)}{v_t^{1/4}} \right\|^2 + \left\| \frac{\bar{\nabla} f(x_t)}{v_t^{1/4}} \right\|^2 - \left\| \frac{\nabla f(\bar{\theta}_t) - \bar{\nabla} f(x_t)}{v_t^{1/4}} \right\|^2 \right). \quad (5)$$

For the last term, by Cauchy-Schwartz inequality,

$$\begin{aligned} \left\| \frac{\nabla f(\bar{\theta}_t) - \nabla \bar{f}(x_t)}{v_t^{1/4}} \right\|^2 &= \left\| \frac{\frac{1}{N} \sum_{i=1}^N (\nabla f_i(\bar{\theta}_t) - \nabla f_i(x_{t,i}))}{v_t^{1/4}} \right\|^2 \\ &\leq \frac{2}{N} \sum_{i=1}^N \left( \left\| \frac{\nabla f_i(\bar{\theta}_t) - \nabla f_i(\bar{x}_t)}{v_t^{1/4}} \right\|^2 + \left\| \frac{\nabla f_i(\bar{x}_t) - \nabla f_i(x_{t,i})}{v_t^{1/4}} \right\|^2 \right). \end{aligned} \quad (6)$$

Using Lipschitz property (Assumption A1) of  $\nabla f_i$ , we can further bound the differences of gradients on RHS of (6) by

$$\frac{2}{N} \sum_{i=1}^N \left\| \frac{\nabla f_i(\bar{\theta}_t) - \nabla f_i(\bar{x}_t)}{v_t^{1/4}} \right\|^2 \leq \frac{2}{N} \sum_{i=1}^N \frac{L \|\bar{\theta}_t - \bar{x}_t\|^2}{\epsilon^{0.5}}, \quad (7)$$

$$\frac{2}{N} \sum_{i=1}^N \left\| \frac{\nabla f_i(\bar{x}_t) - \nabla f_i(x_{t,i})}{v_t^{1/4}} \right\|^2 \leq \frac{2}{N} \sum_{i=1}^N \frac{L \|\bar{x}_t - x_{t,i}\|^2}{\epsilon^{0.5}}. \quad (8)$$

It remains to bound  $\|\bar{\theta}_t - \bar{x}_t\|^2$  and  $\|\bar{x}_t - x_{t,i}\|^2$  using the update rule of  $x$  and  $\theta$ . For the difference between  $\bar{\theta}_t$  and  $\bar{x}_t$ , we have

$$\begin{aligned} \sum_{i=1}^N \|\bar{\theta}_t - \bar{x}_t\|^2 &= \frac{\beta_1^2}{(1-\beta_1)^2} \sum_{i=1}^N \|\bar{x}_t - \bar{x}_{t-1}\|^2 \\ &= \frac{\beta_1^2}{(1-\beta_1)^2} \alpha^2 N \left\| \frac{\bar{m}_{t-1}}{\sqrt{v_{t-1}}} \right\|^2 \leq \frac{\beta_1^2}{(1-\beta_1)^2} \alpha^2 N d \frac{G^2}{\epsilon}. \end{aligned} \quad (9)$$

For the consensus error (8), let  $[t]_k$  be the largest multiple of  $k$  that is less than  $t$ . By the updating rule, we have

$$\sum_i \|\bar{x}_t - x_{t,i}\|^2 = \alpha^2 \sum_{i=1}^N \left\| \sum_{l=[t]_k+1}^{t-1} \left( \frac{m_{l,i}}{\sqrt{v_l}} - \frac{1}{N} \sum_{o=1}^N \frac{m_{l,o}}{\sqrt{v_l}} \right) \right\|^2 \leq 4N(k-1)^2 \alpha^2 d \frac{G^2}{\epsilon}, \quad (10)$$

since  $(v_o)_j \geq \epsilon, \forall j \in [d], o \in [N]$ , and  $\|m_{t,o}\|_\infty \leq G, \forall t, o$ . Combining (6), (7), (8), (9) and (10) gives

$$\left\| \frac{\nabla f(\bar{\theta}_t) - \nabla \bar{f}(x_t)}{v_t^{1/4}} \right\|^2 \leq \frac{\alpha^2 L d G^2}{\epsilon^{1.5}} \left( \frac{2\beta_1^2}{(1-\beta_1)^2} + 8(k-1)^2 \right). \quad (11)$$

Now, combining (5), (11), (4) and (3), telescoping summation gives

$$\begin{aligned} \frac{1}{T} \sum_{t=1}^T \mathbb{E} \left[ \frac{1}{2} \left\| \frac{\nabla f(\bar{\theta}_t)}{v_t^{1/4}} \right\|^2 + \frac{1}{2} \left\| \frac{\nabla \bar{f}(x_t)}{v_t^{1/4}} \right\|^2 \right] &\leq \frac{\mathbb{E}[f(\bar{z}_1)] - \mathbb{E}[f(\bar{z}_{T+1})]}{T\alpha} + \underbrace{\frac{L}{2} \frac{1}{T\alpha} \sum_{t=1}^T \mathbb{E}[\|\bar{\theta}_{t+1} - \bar{\theta}_t\|^2]}_{A_1} \\ &\quad + \underbrace{\frac{1}{T} \sum_{t=1}^T \mathbb{E} \left[ \left\langle \nabla f(\bar{\theta}_t), \frac{\beta_1}{1-\beta_1} \left( \frac{1}{\sqrt{v_{t-1}}} - \frac{1}{\sqrt{v_t}} \right) \odot \bar{m}_{t-1} \right\rangle \right]}_{A_2} \\ &\quad + \alpha^2 \frac{L d G^2}{\epsilon^{1.5}} \left( \frac{\beta_1^2}{(1-\beta_1)^2} + 4(k-1)^2 \right). \end{aligned} \quad (12)$$

To bound  $A_1$ , by (2), we know that

$$\|\bar{\theta}_{t+1} - \bar{\theta}_t\|^2 \leq 2\alpha^2 \left( \left\| \frac{\beta_1}{1-\beta_1} \left( \frac{1}{\sqrt{v_{t-1}}} - \frac{1}{\sqrt{v_t}} \right) \odot \bar{m}_{t-1} \right\|^2 + \left\| \frac{\bar{g}_t}{\sqrt{v_t}} \right\|^2 \right).$$

In addition, conditioned on the  $\sigma$ -field  $\mathcal{F}_{t-1}$  (until  $t-1$ ), we have

$$\begin{aligned} \mathbb{E} \left[ \left\| \frac{\bar{g}_t}{\sqrt{v_t}} \right\|^2 \right] &= \frac{1}{N^2} \mathbb{E} \left[ \sum_{j=1}^N \sum_{i=1}^N \left\langle \frac{g_{t,i}}{\sqrt{v_t}}, \frac{g_{t,j}}{\sqrt{v_t}} \right\rangle \right] \\ &\stackrel{(a)}{=} \frac{1}{N^2} \mathbb{E} \left[ \sum_{j=1}^N \sum_{i=1}^N \left\langle \frac{\nabla f_i(x_{t,i}) + \xi_{t,i}}{\sqrt{v_t}}, \frac{\nabla f_j(x_{t,j}) + \xi_{t,j}}{\sqrt{v_t}} \right\rangle \right] \\ &\stackrel{(b)}{=} \frac{1}{N^2} \left\| \frac{\sum_{i=1}^N \nabla f_i(x_{t,i})}{\sqrt{v_t}} \right\|^2 + \frac{1}{N^2} \sum_{i=1}^N \mathbb{E} \left[ \left\| \frac{\xi_{t,i}}{\sqrt{v_t}} \right\|^2 \right] \stackrel{(c)}{\leq} \left\| \frac{\nabla f(x_t)}{\sqrt{v_t}} \right\|^2 + \frac{1}{N\epsilon} \sigma^2. \end{aligned}$$

where (a) is a decomposition of stochastic gradient, and (b) and (c) are due to **A2**. Furthermore, by **A3** we have

$$\begin{aligned} \mathbb{E} \left[ \sum_{t=1}^T \left\| \frac{\beta_1}{1-\beta_1} \left( \frac{1}{\sqrt{v_{t-1}}} - \frac{1}{\sqrt{v_t}} \right) \odot \bar{m}_{t-1} \right\|^2 \right] &\leq \mathbb{E} \left[ \sum_{t=1}^T \frac{\beta_1^2}{(1-\beta_1)^2} G^2 \frac{1}{\epsilon^{0.5}} \sum_{j=1}^d \left| \frac{1}{\sqrt{(v_{t-1})_j}} - \frac{1}{\sqrt{(v_t)_j}} \right| \right] \\ &\leq \frac{\beta_1^2 G^2 M d T^\gamma}{\epsilon^{0.5} (1-\beta_1)^2}. \end{aligned}$$

Combining above results, we obtain

$$A_1 \leq 2\alpha^2 \sum_{t=1}^T \mathbb{E} \left[ \left\| \frac{\nabla f(x_t)}{\sqrt{v_t}} \right\|^2 + \frac{1}{N\epsilon} \sigma^2 \right] + 2\alpha^2 \frac{\beta_1^2 G^2 M d T^\gamma}{\epsilon^{0.5} (1-\beta_1)^2}.$$

We can use similar argument to get  $A_2 \leq \frac{\beta_1^2 G^2 M T^\gamma}{(1-\beta_1)^2}$ . Returning to (12), since  $z_1 = x_1$ , we have

$$\begin{aligned} \frac{1}{T} \sum_{t=1}^T \mathbb{E} \left[ \frac{1}{2} \left\| \frac{\nabla f(\bar{\theta}_t)}{v_t^{1/4}} \right\|^2 + \frac{1}{2} \left\| \frac{\nabla f(x_t)}{v_t^{1/4}} \right\|^2 \right] &\leq \frac{\mathbb{E}[f(\bar{x}_1)] - \mathbb{E}[f(\bar{z}_{T+1})]}{T\alpha} + \frac{L}{T} \alpha \sum_{t=1}^T \mathbb{E} \left[ \left\| \frac{\nabla f(x_t)}{\sqrt{v_t}} \right\|^2 + \frac{1}{N\epsilon} \sigma^2 \right] \\ &\quad + \frac{1}{T^{1-\gamma}} \frac{\beta_1^2 G^2 M d}{(1-\beta_1)^2} + \frac{\alpha L}{T^{1-\gamma}} \frac{\beta_1^2 G^2 M d}{\epsilon^{0.5} (1-\beta_1)^2} + \alpha^2 \frac{L d G^2}{\epsilon^{1.5}} \left( \frac{\beta_1^2}{(1-\beta_1)^2} + 4(k-1)^2 \right). \end{aligned}$$

By choosing  $\alpha = \min(\frac{\sqrt{N}}{\sqrt{Td}}, \frac{\sqrt{\epsilon}}{4L})$ , we have

$$\frac{L}{T} \alpha \sum_{t=1}^T \mathbb{E} \left[ \left\| \frac{\nabla f(x_t)}{\sqrt{v_t}} \right\|^2 \right] \leq \frac{1}{4} \frac{1}{T} \sum_{t=1}^T \mathbb{E} \left[ \left\| \frac{\nabla f(x_t)}{v_t^{1/4}} \right\|^2 \right].$$

Let  $\Delta = \mathbb{E}[f(\bar{x}_1)] - \min_x f(x)$ , we obtain

$$\begin{aligned} \frac{1}{T} \sum_{t=1}^T \mathbb{E} \left[ \frac{1}{2} \left\| \frac{\nabla f(\bar{\theta}_t)}{v_t^{1/4}} \right\|^2 + \frac{1}{4} \left\| \frac{\bar{\nabla} f(x_t)}{v_t^{1/4}} \right\|^2 \right] &\leq \frac{\sqrt{d}\Delta}{\sqrt{TN}} + \frac{L\sqrt{d}}{\sqrt{TN}} \sigma^2 \frac{1}{\epsilon} + \frac{1}{T^{1-\gamma}} \frac{\beta_1^2 G^2 M d}{(1-\beta_1)^2} \\ &+ \frac{\sqrt{NL}}{T^{1.5-\gamma}} \frac{\beta_1^2 G^2 M \sqrt{d}}{\epsilon^{0.5}(1-\beta_1)^2} + \frac{NLG^2}{T\epsilon^{1.5}} \left( \frac{\beta_1^2}{(1-\beta_1)^2} + 4(k-1)^2 \right). \end{aligned}$$

Note that by C-S and Jensen's inequality,

$$\begin{aligned} \left\| \frac{\bar{\nabla} f(x_t)}{v_t^{1/4}} \right\|^2 &\geq \frac{1}{2} \left\| \frac{\nabla f(\bar{x}_t)}{v_t^{1/4}} \right\|^2 - \left\| \frac{\bar{\nabla} f(x_t) - \nabla f(\bar{x}_t)}{v_t^{1/4}} \right\|^2 \\ &\geq \frac{1}{2} \left\| \frac{\nabla f(\bar{x}_t)}{v_t^{1/4}} \right\|^2 - \frac{1}{N} \sum_{i=1}^N \left\| \frac{\nabla f_i(x_{t,i}) - \nabla f_i(\bar{x}_t)}{v_t^{1/4}} \right\|^2 \\ &\geq \frac{1}{2} \left\| \frac{\nabla f(\bar{x}_t)}{v_t^{1/4}} \right\|^2 - 4L(k-1)^2 \alpha^2 d \frac{G^2}{\epsilon^{1.5}}. \end{aligned}$$

The desired result then follows. This completes the proof.  $\square$

## 5 Experimental Evaluation

The objective of the experimental evaluation is to investigate the performance of our system and the impact of optimizations:

- What are the impacts of our proposed optimizations, including two-phase GPU communication, GPUDirect RDMA, SSD direct I/O, and core binding?
- Does  $k$ -step model merging hurt the prediction accuracy?
- How much data communication time is saved?

**System.** We perform the experimental evaluation on 8 GPU computing nodes. Each node has 8 cutting-edge 32 GB HBM GPUs, server-grade CPUs with 48 cores (96 threads),  $\sim 1$  TB of memory,  $\sim 20$  TB RAID-0 NVMe SSDs and a 100 Gb RDMA network adaptor. Thus, in our setting, using  $n$  nodes corresponds to  $8 \times k$  local distributed workers. All nodes are inter-connected through a high-speed Ethernet switch. We use a web search CTR prediction model in real-world online sponsor advertising applications to investigate the effectiveness of our proposed system. The number of sparse parameters is  $\sim 10^{11}$ . The number of dense parameters is  $\sim 10^6$ . The size of the model is  $\sim 10$  TB. For dense parameters, we use Adam (Kingma and Ba, 2015) optimizer. For sparse parameters, we use AdaGrad optimizer (Duchi et al., 2011) to avoid storing the extra first-order momentum which would take substantial space for the huge sparse layers. Since each training input only leads to a small number of non-zero gradients in the sparse layers, we adopt a standard distributed setting on sparse model parameters, where the gradients are averaged for update in every iteration. This is cheap in communication. For dense model that takes more communication, we use  $k$ -step Adam as optimizer, with default parameter setting  $\beta_1 = 0.0$ ,  $\beta_2 = 0.999$ .

**Data.** We collect user click history logs from a real-world search engine in 24 hours as the training and testing dataset. The dataset is chunked into batches—each batch contains  $\sim 4 \times 10^6$  instances. The worker further splits each batch into mini-batches with  $\sim 1,000$  instances as a training step. Note that our “ $k$ -step” is worked on a mini-batch level: the model merging is performed after every  $k$  mini-batches. The training and testing are performed in an online learning fashion: an instance is first predicted using the inference result of the current model to generate the test accuracy, and then it is fed to the model for the training. The online training is “hot-started”: we use the trained model on previous days at the start point in the experiments instead of a random initialized one.

## 5.1 Core Binding and SSD Direct I/O

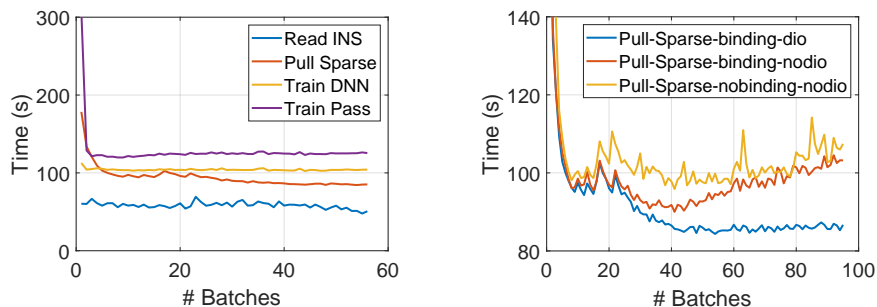


Figure 5: Left: Time distribution of CTR model training with all optimizations; Right: Time of pull sparse parameters with/without core binding and direct I/O.

Figure 5 illustrates the effect of using core binding and direct I/O on SSDs. The experiments are executed in one single node to eliminate the impact of the network communications. In the left part of the figure, we present the training time with core binding and direct I/O for each stage, where **Read Ins** is the time to read and parse training instances from the network file system; **Pull Sparse** is the time to load sparse parameters from main memory and SSDs to GPUs; **Train DNN** is the GPU computation time to perform feed forward and backward propagation; **Overall** is the overall execution time to train a batch. The overall time is not the summation of all three stages (Read Ins, Pull Sparse, and Train DNN) because the three stages are executed in a pipeline—the execution time of these stages are overlapped. With core binding and direct I/O, the sparse parameter loading becomes faster than the DNN training and no longer a bottleneck. The right part of Figure 5 presents the finer granularity comparison for core binding and direct I/O. These two techniques mainly optimize the **Pull Sparse** stage. Thus, we compare the execution time of pulling sparse parameters by disabling them. **Pull-binding-dio** is the configuration enabling both optimizations. Note that **Pull-binding-dio** is the same curve as the **Pull-Sparse** in the left part of the figure. The range of the y axis is magnified and more batch training is presented to show the detailed optimization impact of binding and direct I/O. **Pull-binding-nodio** and **Pull-nobinding-nodio** illustrate the configuration when we disable direct I/O and disable both core binding and direct I/O, respectively. The core binding provides 5 – 10% improvement to the baseline scenario. Adding the direct I/O on SSDs shows another 10 – 20% improvement. The in-memory cache management maintains the frequently used parameters well during the training progress. The direct I/O improvement becomes larger in the late stage of the training because it eliminates the more unnecessary operating system level page cache I/Os.

## 5.2 GPU Communications

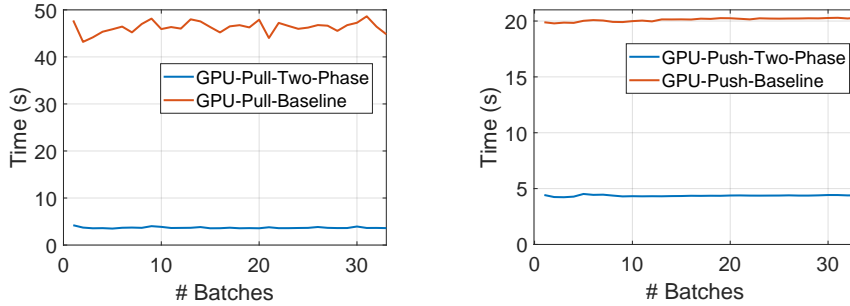


Figure 6: Time of pull/push operations in GPU HBM with/without two-phase GPU communication.

**Two-Phase GPU Communication.** The two-phase GPU communication technique uses a middleman GPU buffer to eliminate the data transfer on PCIe and main memory. Figure 6 presents the GPU communications within a node to pull the parameters in the distributed GPU hash table from the HBM of peer GPUs (GPU-Pull); and the time to update the parameters in the distributed GPU hash table (GPU-Push). As depicted in Figure 6, the two-phase optimization reduces as much as 90% communication time among GPUs in the same node for pulling parameters and 75% improvement for pushing updates to other peer GPUs.

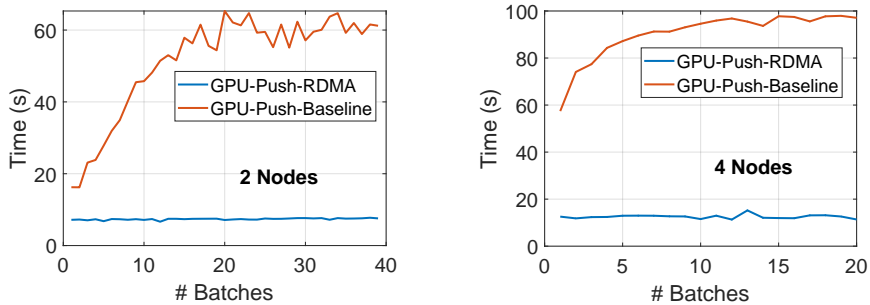


Figure 7: Time of push operations with/without RDMA.

**GPUDirect RDMA.** Figure 7 shows the push communications time for 2 and 4 nodes. We fix the total training data the same. With more workers introduced in more nodes, the total #Batches is reduced. Therefore, the figure shows 40 batches for 2 nodes and 20 batches for 4 nodes. As expected, the communications increase when more nodes are involved. The GPUDirect RDMA enables GPUs to communicate with GPUs on other nodes without involving CPUs. It reduces as much as 87% communications for 2-node setting and 84% for the 4-node case. As a result of the communication time reduction, the overall training time is reduced 54% (Figure 8).

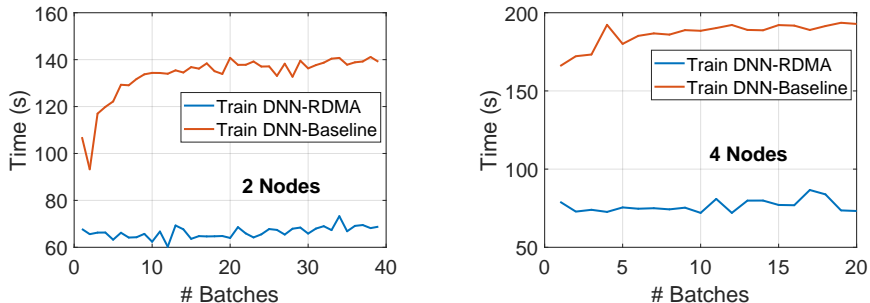


Figure 8: Time of overall DNN training with/without RDMA.



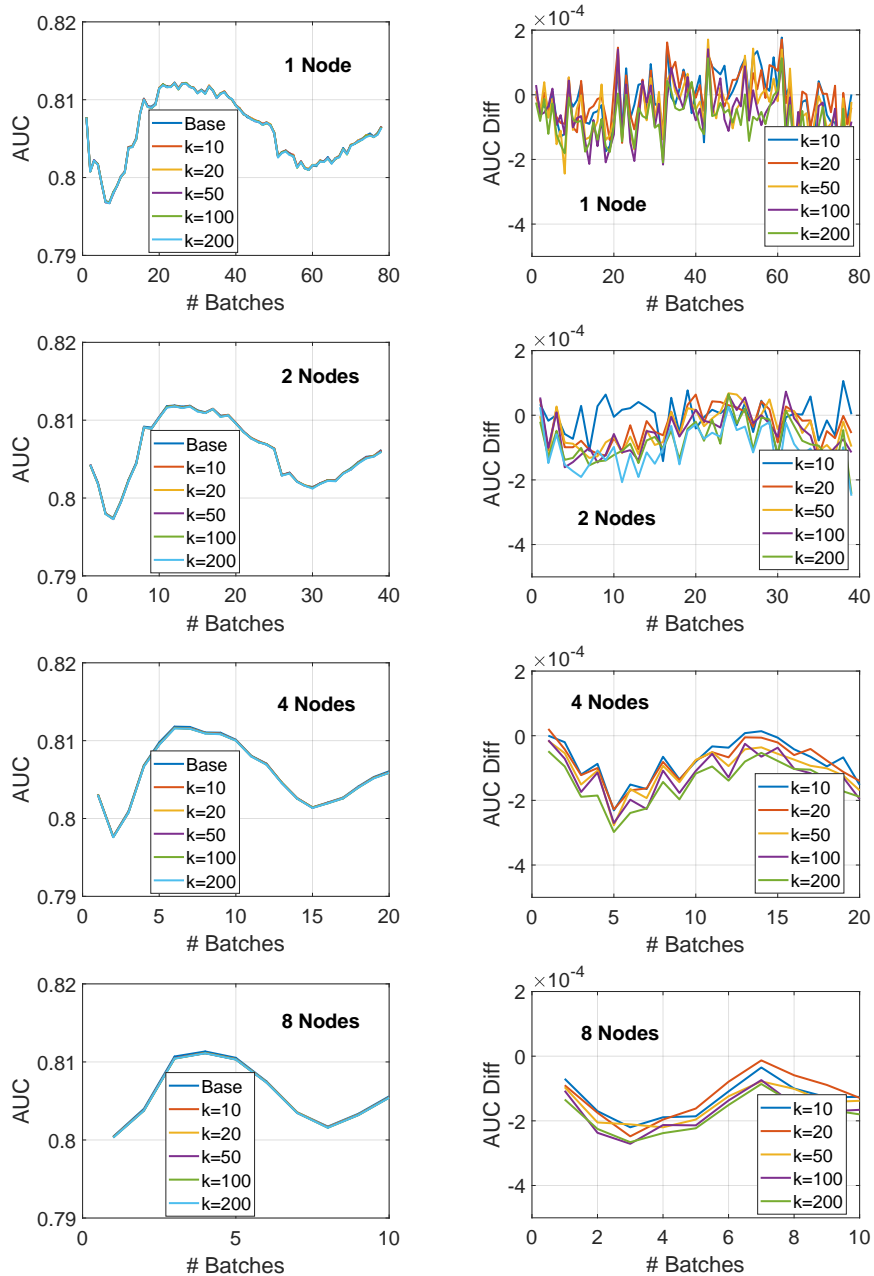


Figure 9:  $k$ -step communication-efficient training. Left: AUC vs. number of training batches. Right: AUC difference of ( $k$ -step - baseline).

### 5.3 Communication of $k$ -Step Model Merging

The optimizations we investigated above only modify the data communication routes, which are lossless. However, the proposed  $k$ -step model merging touches the training algorithm. In this section, we evaluate our proposed  $k$ -step model merging algorithm in two measures: (a) accuracy; and (b) execution time.

**Accuracy.** The CTR prediction accuracy is one of the most critical measures for industry advertising applications. We have to guarantee no noticeable accuracy drop when we apply any optimizations. Here we employ Area Under the Curve (Huang and Ling, 2005) (AUC) as the quality measure of our trained models. Figure 9 depict the AUC for 1, 2, 4, and 8 node settings. The right part of the figure is a zoomed-in view of the left part. When we vary the  $k$  from 10 to 200, almost no differences in AUC can be observed in the left part of the figure. In the online learning context, it is normal to observe a higher AUC in working hours since there are more training instances in those hours—the model can better predict the user behaviors in that time period. In the zoomed-in view, we can observe that the AUC diff vibrates within 0.0002% range in most settings. We can assume the AUC loss is minimal and statistically ignorable.

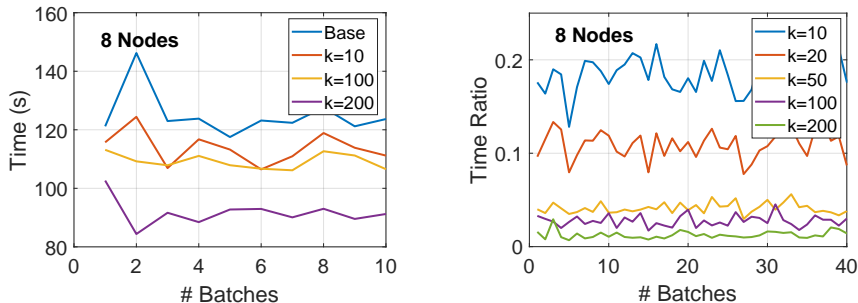


Figure 10: Left: time of DNN training with  $k$ -step communication scheme. Right: Communication time (model transmission) ratio of  $k$ -step over baseline. The average ratio is 18.1%, 10.8%, 6.4%, 2.8% and 1.2%, for  $k = 10, 20, 50, 100, 200$ .

**Execution time.** Figure 10 reports the overall execution time to train the model with/without  $k$ -step model merging on 8 nodes. We can reduce as much as 25% execution time when  $k = 200$ . The right part of the figure presents the communication time ratio of  $k$ -step over the baseline case (all optimizations except  $k$ -step). The communication time is approximately linearly reduced as we increase  $k$ . The overall execution time is not proportionally reduced because the training system is executed in a pipeline—there is synchronization overhead with other stages.

### 5.4 Discussion

Now we can answer the questions driven the experimental evaluation. Our proposed core binding and SSD I/O improve the sparse parameter pulling stage around 15%. For inner-node GPU communication, our two-phase GPU communication algorithm reduces around 90% GPU communication time. For the inter-node case, our GPUDirect RDMA optimization cuts the communication cost to 1/6 and 1/8 for 2-node and 4-node settings, respectively. In terms of accuracy, through 1-node to 8-node different scenarios, our proposed  $k$ -step merging algorithm is able to generate almost the same accurate result comparing with the original optimizer—the AUC diff is within 0.0002% range. Meanwhile, our proposed training framework is more than 4X faster to finish the training execution.

## 6 Conclusion

In this paper, we propose a hardware-aware training workflow that couples the hardware topology into the algorithm design to improve the communication bandwidth between devices. To reduce the extensive communication between computing nodes, we introduce a  $k$ -step model merging algorithm for Adam and theoretically provide its convergence rate in non-convex optimization. We evaluate the proposed system on real-world ads data. The empirical results show that our proposed optimizations improve both the inner-node communication bandwidth and the inter-node communication. The experimental evaluation confirms that our proposed training framework achieves better execution time while maintaining the same test accuracy.

## References

- Andrei Broder. A taxonomy of web search. *SIGIR Forum*, 36(2):3–10, 2002.
- Xiangyi Chen, Sijia Liu, Ruoyu Sun, and Mingyi Hong. On the convergence of A class of adam-type algorithms for non-convex optimization. In *Proceedings of the 7th International Conference on Learning Representations (ICLR)*, New Orleans, LA, 2019.
- Xiangyi Chen, Xiaoyun Li, and Ping Li. Toward communication efficient adaptive gradient method. In *Proceedings of the 2020 ACM-IMS on Foundations of Data Science Conference (FODS)*, pages 119–128, 2020.
- Heng-Tze Cheng, Levent Koc, Jeremiah Harmsen, Tal Shaked, Tushar Chandra, Hrishu Aradhye, Glen Anderson, Greg Corrado, Wei Chai, Mustafa Ispir, Rohan Anil, Zakaria Haque, Lichan Hong, Vihan Jain, Xiaobing Liu, and Hemal Shah. Wide & deep learning for recommender systems. In *Proceedings of the 1st Workshop on Deep Learning for Recommender Systems, (DLRS@RecSys)*, pages 7–10, Boston, MA, 2016.
- Paul Covington, Jay Adams, and Emre Sargin. Deep neural networks for youtube recommendations. In *Proceedings of the 10th ACM Conference on Recommender Systems (RecSys)*, pages 191–198, Boston, MA, 2016.
- Henggang Cui, James Cipar, Qirong Ho, Jin Kyu Kim, Seunghak Lee, Abhimanu Kumar, Jinliang Wei, Wei Dai, Gregory R. Ganger, Phillip B. Gibbons, Garth A. Gibson, and Eric P. Xing. Exploiting bounded staleness to speed up big data analytics. In *Proceedings of the 2014 USENIX Annual Technical Conference (USENIX ATC)*, pages 37–48, Philadelphia, PA, 2014.
- Henggang Cui, Hao Zhang, Gregory R. Ganger, Phillip B. Gibbons, and Eric P. Xing. Geeps: Scalable deep learning on distributed GPUs with a GPU-specialized parameter server. In *Proceedings of the Eleventh European Conference on Computer Systems (EuroSys)*, pages 4:1–4:16, London, UK, 2016.
- John C. Duchi, Elad Hazan, and Yoram Singer. Adaptive subgradient methods for online learning and stochastic optimization. *J. Mach. Learn. Res.*, 12:2121–2159, 2011.
- Benjamin Edelman, Michael Ostrovsky, and Michael Schwarz. Internet advertising and the generalized second-price auction: Selling billions of dollars worth of keywords. *American economic review*, 97(1):242–259, 2007.

- Daniel C. Fain and Jan O. Pedersen. Sponsored search: A brief history. *Bulletin of the American Society for Information Science and Technology*, 32(2):12–13, 2006.
- Miao Fan, Jiacheng Guo, Shuai Zhu, Shuo Miao, Mingming Sun, and Ping Li. MOBIUS: towards the next generation of query-ad matching in baidu’s sponsored search. In *Proceedings of the 25th ACM SIGKDD International Conference on Knowledge Discovery & Data Mining, (KDD)*, pages 2509–2517, Anchorage, AK, 2019.
- Denis Foley and John Danskin. Ultra-performance pascal GPU and nvlLink interconnect. *IEEE Micro*, 37(2):7–17, 2017.
- Thore Graepel, Joaquin Quiñonero Candela, Thomas Borchert, and Ralf Herbrich. Web-scale bayesian click-through rate prediction for sponsored search advertising in microsoft’s bing search engine. In *Proceedings of the 27th International Conference on Machine Learning (ICML)*, pages 13–20, Haifa, Israel, 2010.
- Huifeng Guo, Ruiming Tang, Yunming Ye, Zhenguo Li, and Xiuqiang He. Deepfm: A factorization-machine based neural network for ctr prediction. In *Proceedings of the Twenty-Sixth International Joint Conference on Artificial Intelligence (IJCAI)*, pages 1725–1731, Melbourne, Australia, 2017.
- Qirong Ho, James Cipar, Henggang Cui, Seunghak Lee, Jin Kyu Kim, Phillip B. Gibbons, Garth A. Gibson, Gregory R. Ganger, and Eric P. Xing. More effective distributed ml via a stale synchronous parallel parameter server. In *Advances in Neural Information Processing Systems (NIPS)*, pages 1223–1231, Lake Tahoe, NV, 2013.
- Jin Huang and Charles X Ling. Using auc and accuracy in evaluating learning algorithms. *IEEE Transactions on Knowledge and Data Engineering (TKDE)*, 17(3):299–310, 2005.
- Yuzhen Huang, Tatiana Jin, Yidi Wu, Zhenkun Cai, Xiao Yan, Fan Yang, Jinfeng Li, Yuying Guo, and James Cheng. Flexps: Flexible parallelism control in parameter server architecture. *Proc. VLDB Endow.*, 11(5):566–579, 2018.
- Diederik P. Kingma and Jimmy Ba. Adam: A method for stochastic optimization. In *Proceedings of the 3rd International Conference on Learning Representations (ICLR)*, San Diego, CA, 2015.
- Mu Li, David G. Andersen, Jun Woo Park, Alexander J. Smola, Amr Ahmed, Vanja Josifovski, James Long, Eugene J. Shekita, and Bor-Yiing Su. Scaling distributed machine learning with the parameter server. In *Proceedings of the 11th USENIX Symposium on Operating Systems Design and Implementation (OSDI)*, pages 583–598, Broomfield, CO, 2014.
- Jianxun Lian, Xiaohuan Zhou, Fuzheng Zhang, Zhongxia Chen, Xing Xie, and Guangzhong Sun. xdeepfm: Combining explicit and implicit feature interactions for recommender systems. In *Proceedings of the 24th ACM SIGKDD International Conference on Knowledge Discovery & Data Mining (KDD)*, pages 1754–1763, London, UK, 2018.
- Liang Luo, Jacob Nelson, Luis Ceze, Amar Phanishayee, and Arvind Krishnamurthy. Parameter hub: a rack-scale parameter server for distributed deep neural network training. In *Proceedings of the ACM Symposium on Cloud Computing (SoCC)*, pages 41–54, Carlsbad, CA, 2018.
- Brendan McMahan, Eider Moore, Daniel Ramage, Seth Hampson, and Blaise Agüera y Arcas. Communication-efficient learning of deep networks from decentralized data. In *Proceedings of the 20th International Conference on Artificial Intelligence and Statistics (AISTATS)*, volume 54, pages 1273–1282, Fort Lauderdale, FL, 2017.

- Yanru Qu, Han Cai, Kan Ren, Weinan Zhang, Yong Yu, Ying Wen, and Jun Wang. Product-based neural networks for user response prediction. In *Proceedings of the IEEE 16th International Conference on Data Mining (ICDM)*, pages 1149–1154, Barcelona, Spain, 2016.
- Sashank J. Reddi, Satyen Kale, and Sanjiv Kumar. On the convergence of adam and beyond. In *Proceedings of the 6th International Conference on Learning Representations (ICLR)*, Vancouver, Canada, 2018.
- Ying Shan, T. Ryan Hoens, Jian Jiao, Haijing Wang, Dong Yu, and J. C. Mao. Deep crossing: Web-scale modeling without manually crafted combinatorial features. In *Proceedings of the 22nd ACM SIGKDD International Conference on Knowledge Discovery and Data Mining (KDD)*, pages 255–262, San Francisco, CA, 2016.
- Leslie G. Valiant. A bridging model for parallel computation. *Commun. ACM*, 33(8):103–111, 1990.
- Zhiqiang Xu, Dong Li, Weijie Zhao, Xing Shen, Tianbo Huang, Xiaoyun Li, and Ping Li. Agile and accurate CTR prediction model training for massive-scale online advertising systems. In *Proceedings of the International Conference on Management of Data (SIGMOD)*, pages 2404–2409, Virtual Event, China, 2021.
- Hao Yu, Rong Jin, and Sen Yang. On the linear speedup analysis of communication efficient momentum SGD for distributed non-convex optimization. In Kamalika Chaudhuri and Ruslan Salakhutdinov, editors, *Proceedings of the 36th International Conference on Machine Learning (ICML)*, volume 97, pages 7184–7193, Long Beach, CA, 2019.
- Weijie Zhao, Jingyuan Zhang, Deping Xie, Yulei Qian, Ronglai Jia, and Ping Li. AIBox: CTR prediction model training on a single node. In *Proceedings of the 28th ACM International Conference on Information and Knowledge Management (CIKM)*, pages 319–328, Beijing, China, 2019.
- Weijie Zhao, Deping Xie, Ronglai Jia, Yulei Qian, Ruiquan Ding, Mingming Sun, and Ping Li. Distributed hierarchical GPU parameter server for massive scale deep learning ads systems. In *Proceedings of Machine Learning and Systems (MLSys)*, Austin, TX, 2020.
- Dongruo Zhou, Yiqi Tang, Ziyang Yang, Yuan Cao, and Quanquan Gu. On the convergence of adaptive gradient methods for nonconvex optimization. *CoRR*, abs/1808.05671, 2018a.
- Fan Zhou and Guojing Cong. On the convergence properties of a k-step averaging stochastic gradient descent algorithm for nonconvex optimization. In *Proceedings of the Twenty-Seventh International Joint Conference on Artificial Intelligence (IJCAI)*, pages 3219–3227, Stockholm, Sweden, 2018.
- Guorui Zhou, Xiaoqiang Zhu, Chengru Song, Ying Fan, Han Zhu, Xiao Ma, Yanghui Yan, Junqi Jin, Han Li, and Kun Gai. Deep interest network for click-through rate prediction. In *Proceedings of the 24th ACM SIGKDD International Conference on Knowledge Discovery & Data Mining (KDD)*, pages 1059–1068, London, UK, 2018b.
- Zhixin Zhou, Shulong Tan, Zhaozhuo Xu, and Ping Li. Möbius transformation for fast inner product search on graph. In *Advances in Neural Information Processing Systems (NeurIPS)*, pages 8216–8227, Vancouver, Canada, 2019.